# Sn/Mn/Bi2O3Ternary Pyrotechnic Time Delay Compositions

Shasha Guo, Walter W. Focke,*and Shepherd M. Tichapondwa

Institute of Applied Materials, Department of Chemical Engineering, University of Pretoria, Hatfield 0028, Pretoria, South Africa

* Corresponding Author

Walter W. Focke - Institute of Applied Materials, Department of Chemical Engineering, University of Pretoria, Private Bag X20, Hatfield 0028, Pretoria, South Africa. Email: walter.focke@up.ac.za

## Abstract

Pyrotechnic compositions are usually employed in time delay detonators to facilitate controlled initiation of explosive charges in mining and quarrying operations. Traditional slow-burning formulations are problematic, as they contain heavy metals which are bio-accumulative and toxic to the environment. A combination of traditional thermite and intermetallic reactions using “green” reagents was therefore investigated as a possible alternative. It was hypothesized that the high thermite reaction temperature would ensure a sustained intermetallic reaction, resulting in the desired slow-burning effect. A ternary composition comprising manganese and tin as fuels mixed with bismuth oxide as an oxidizer was used to explore this concept. Burn rates ranging from 2.9 to 10.9 mm·s$^{-1}$ were obtained and were dependent on the relative proportions of the reagents. Burn rate predictions, using a Padè mixture model, were in close agreement with the measured data. The reaction products consisted of mixtures of metal oxides, manganese stannate, and $Mn_3Sn$, which was the only intermetallic formed. The slowest burning compositions were those associated with the formation of this intermetallic compound.

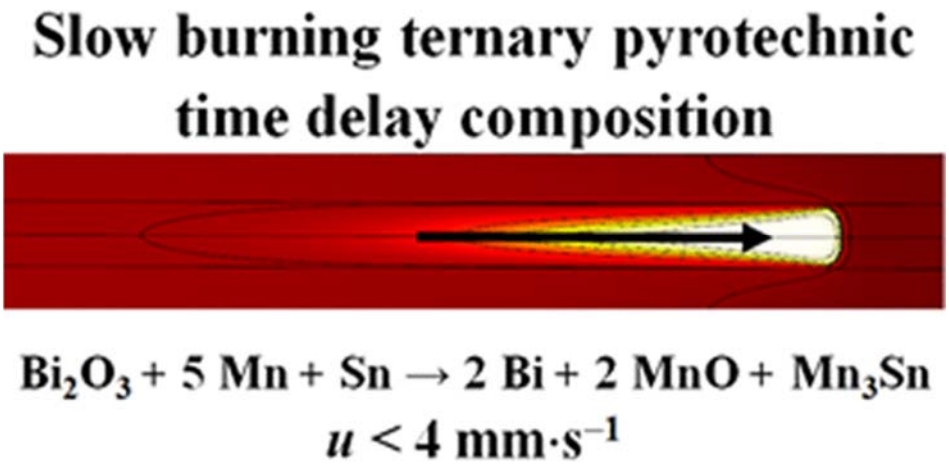


KEYWORDS: Environmentally benign; Pyrotechnic time delays; Thermites; Bismuth oxide; Tin; Manganese

## Introduction

Conventional pyrotechnics are based on intimate mixtures of two or more powders capable of a highly exothermic, self-sustaining reaction.[1,2] Ignition requires an external energy impulse that rapidly heats the mixture to a very high temperature.[3] Once ignited, a steep reaction front develops that propagates through the mixture as it converts the reactants into products. The reaction front will be relatively sharp and self-sustaining provided both the heat of reaction and the activation energy feature high values.[4]

In mining and quarrying operations, time delay detonators are employed to facilitate controlled initiation of explosive charges in a pattern of boreholes.[5,6] The timing of the sequential initiation events is carefully chosen in order to control the fragmentation and throw of the rock being blasted and to reduce ground vibration as well as air blast noise.[6] Both chemical and electronic time delay detonators are used, but the simplicity, ruggedness, and low cost of pyrotechnic delays make them particularly attractive for high volume mining applications. Figure 1 shows, schematically, a typical pyrotechnic time delay detonator. The delay element itself typically consists of a metal tube that holds the compressed-powder time delay composition.

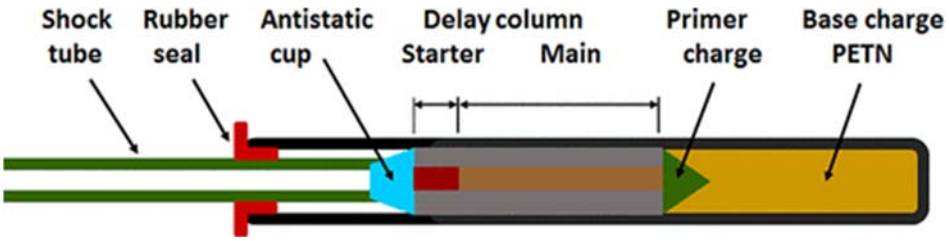


**Figure 1.** Schematic illustration of a typical pyrotechnic time delay detonator.

In order to achieve either short or long time delay in a fixed-length delay element, a range of slow- to fast-burning compositions is necessary. The former is the primary interest of this article with a target set at burning rates in glass tubes of less than 5 $mm \cdot s^{-1}$.

Time delay pyrotechnic compositions are usually compacted into small-diameter tubes. The transmission of the initiation impulse must occur in a precisely adjustable time interval. Thus, compositions that burn at a constant, predetermined rate in an essentially gasless fashion are preferred.[7] The actual time delay realized is determined by the nature of the reactants, the stoichiometry of the composition, the dimensions of the column, and the material of construction of the tube walls.[5,8] The thermal diffusivity of the mixture is always important as flame propagation depends on reignition of adjacent layers along the burning path. Furthermore, good mixing and adequate particle–particle contact between reactants (i.e., efficient particle packing) is a prerequisite for stable and reproducible burning.

Numerous pyrotechnic time delay compositions, comprising mixtures of fuels and oxidizers, have been developed for different applications.[9] Some commercial pyrotechnic

compositions contain heavy-metal-based oxidizers, e.g., lead oxides, barium sulfate, or chromates. Such compounds are deemed environmentally unfriendly and pose a potential health hazard.[10] This has led to the tightening of health and safety legislation and concerted efforts to find "green" replacements.[11–13] However, for the time being, commercial mine detonators continue to rely on heavy metal-based pyrotechnic time delays. It seems that, despite significant efforts to find greener replacements, cost-effective alternatives remain elusive. It could be that acceptable solutions may require the exploration of new concepts. Possibilities are offered by systems that combine the classic thermite with other self-heat sustained reactions, e.g., intermetallic reactions or reactions between different oxides.

Thermites are pyrotechnic compositions that produces high heat via a strongly exothermic reaction. Thermites employ metal fuel powders with high volumetric and gravimetric combustion enthalpies (e.g., Al, Mg, Mn, etc.) and metal-oxide oxidants such as $Fe_2O_3$, CuO, NiO, $MoO_3$, etc. On combustion, the metal oxide is reduced to its metal state by the less noble metallic fuel which, in turn, is converted into a more stable metal oxide.

The high reaction temperature achieved with thermites precludes their direct use in conventional pyrotechnic time delay systems. It frequently far exceeds the melting point of the detonator subassemblies causing premature failure. On the other hand, the exothermicity of intermetallic reactions often proves insufficient to sustain reliable burning in time delay columns. Combining the two approaches may provide a solution to both problems.[14–16] The dilution effect posed by the intermetallic component provides the desired reduction in the overall reaction temperature. Furthermore, adding a carefully chosen thermite may boost the exothermicity of the intermetallic, and thereby facilitate reliable burning. Analysis of the burning rate in cylindrical tubes suggests that a slow burning rate requires a composition characterized by a reaction with a very large activation energy and a relatively low exothermicity.[9] The last aspect favors the application of intermetallic systems. The main objective of the thermite portion should therefore be to provide sufficient heat to guarantee reliable burning without materially increasing the burning rate.

The less toxic heavy metals include copper, tin, tungsten, and bismuth, and probably manganese. Both tin and bismuth are nonessential metals, as they have no established biological function.[10] Nevertheless, inorganic tin compounds exhibit a very low toxicity in animals mainly due to a generally low water solubility, poor absorption, and a low tendency for accumulation in tissues and rapid excretion.[17] Bismuth is a remarkably harmless element among the toxic heavy metals.[18] The low toxicity of most inorganic bismuth compounds is attributed to their insolubility that prevents absorption.[18,19] Furthermore, inorganic bismuth salts possess demulcent qualities, i.e., they protect mucous membranes by forming protective films that relieve irritation. Bismuth is therefore considered to be an eco-friendly metal with a status of a "green element".[17] These attributes motivated the exploration of combinations of bismuth oxide (as oxidizer) with tin and manganese (as fuels) for their potential in slow-burning time delay applications. Detailed results for the $Bi_2O_3$/Mn binary, and the thermochemistry of the $Bi_2O_3$/Sn binary, have already been reported elsewhere.[16,20] Therefore, this article focuses on the behavior of the ternary system.

**Table 1. Characteristics of the Raw Material Powders**

| Powder | Supplier | Particle size[a] ($\mu$m) | | | BET[b] ($m^2\ g^{-1}$) | Density ($g\ cm^{-3}$) |
|---|---|---|---|---|---|---|
| | | $D_{10}$ | $D_{50}$ | $D_{90}$ | | |
| Sn | Sigma-Aldrich | 2.01 ± 0.04 | 4.25 ± 0.08 | 8.20 ± 0.27 | 0.34 | 7.625 |
| Mn | Atlantic Equipment Engineers | 9.19 ± 0.12 | 24.6 ± 0.3 | 51.7 ± 0.78 | 0.29 | 7.21 |
| $Bi_2O_3$ | Hunan JinWang Bismuth Industry Co Ltd., China | 3.08 ± 0.04 | 7.48 ± 0.09 | 17.6 ± 0.67 | 0.53 | 8.90 |

[a]Volume-based mean particle size ±1 SD. [b]BET surface area.

## Experimental Section

### Materials

Table 1 lists the suppliers and some of the key characteristics of the neat powders employed. All materials were used as received without further processing.

### Preparation Methods

Binary mixtures were prepared by combining the bismuth oxide with the desired fuel. Additionally, four sets of binary base mixtures, corresponding to the compositions listed in Table 2, were made first. They were combined in different proportions to make up the ternary mixtures. All these compositions were prepared by a brush mixing technique. Weighed-out reagent quantities were combined and repeatedly brushed through a 45 µm sieve. This operation was repeated for the ternary samples that required combining the base mixture among themselves, or with neat fuel powders in preselected proportions.

**Table 2. Binary Components of the Different Base Mixtures[a]**

| Powder/Group | A | B | C | D |
|---|---|---|---|---|
| $Bi_2O_3$ | 72.35 | 70.0 | 55.0 | - |
| Mn | - | - | 45.0 | 18.79 |
| Sn | 27.65 | 30.0 | - | 81.21 |

[a]Values are given in wt %.

The well-mixed formulations were loaded into 50-mm-long borosilicate glass tubes with inside and outside diameters of 6.0 mm and 8.0 mm, respectively. The tubes were closed at one end using a small portion of Prestik putty. Small increments of the mixed powders (75 ± 5 mg) were dispensed into the tubes. The loaded powder portion was consolidated, by repeated tapping, before adding the next increment. The final loading was 4.2 ± 0.3 g at 48 ± 2% TMD.

Samples burned in lead tubes were prepared in a similar fashion. Only four compositions were tested in this way. The starting lead tube lengths were 155 mm with OD = 11.5 mm and ID 7.0 mm. Composition amounts weighing 16.0 ± 0.6 g were tap-filled in the tube with the one end sealed by a crimp. The compositions in the tubes were consolidated by applying a series of three consecutive rolling operations on a proprietary tube-rolling machine. During each rolling operation, the sealed tube was passed through a hole with a smaller diameter. The fully compacted sample tubes featured outer diameters of 10.0 mm with the inner diameters reduced to 6.0 mm. The rolled lead tubes were then cut to a standard length of 38 ± 2 mm to form the delay elements.

### Burning Rate Measurements

The compacted lead tubes were clamped in a horizontal position. The filled glass tubes were placed inside other, slightly larger, glass tubes that served as horizontal holders. Ignition was effected by placing the tip of a sparkler against the one end of the delay element and igniting it at the other end. At the moment of ignition of the actual delay column, a yellow "cloud" appeared. For the burns inside lead tubes, the end of the burn was taken as the point when the flame emerged on the other side. The burning events were recorded with a

digital camera at a frame rate of 240 Hz. The burning rate was estimated from the burn time, extracted from the video recording, and the effective burn length.

### Characterization

The morphology of the powder particles was studied with a Zeiss Ultra Plus 55 scanning electron microscope (SEM) fitted with an In-Lens detector. The voltage setting was either 1 kV or 5 kV. The powders were carbon-coated with an Emitech K950X coater before scanning.

Particle size distributions and BET surface areas of the raw materials were determined with a Malvern Mastersizer 3000 and with a Micromeritics TriStar II 3020, respectively.

The burn residue slags were milled into fine powders using a tungsten carbide mill. The samples for XRD were prepared according to the standardized Panalytical backloading system, which provides a nearly random distribution of the particles. The samples were analyzed using a PANalytical X'Pert Pro powder diffractometer in θ–θ configuration with an X'Celerator detector and variable divergence and fixed receiving slits with Fe filtered Co Kα radiation (λ = 1.789 Å). The mineralogy was determined by selecting the best-fitting pattern from the ICSD database compared to the measured diffraction pattern, using X'Pert Highscore plus software. The relative phase amounts (weight% of crystalline portion) were estimated using the Rietveld method (X'Pert Highscore plus software).

X-ray fluorescence spectroscopy (XRF) analysis was performed on the bismuth oxide powder. A sample was roasted at 1000 °C and a sample mass of 1 g of the residue was fused with about 6 g of lithium tetraborate at 1050 °C for metal oxide determination.

Energy output measurements, of selected compositions, were conducted in a Parr 6200 bomb calorimeter. A proprietary starter (200 mg), with known energy output, was used to initiate the Mn–$Bi_2O_3$ samples, weighing between 2 and 3 g. For the Sn–$Bi_2O_3$ mixtures, the sample size was between 5 and 6 g and no starter was employed. Ignition was accomplished with an electrically heated 30-gauge nichrome wire initiator. The tests were conducted in an inert helium atmosphere at a starting pressure of 3.0 MPa. Measurement were carried out in triplicate. The reported results were corrected for the effect contributed by the starter.

## Results and Discussion

### Powder Characterization

Scanning electron microscopy (SEM) images of the neat particles are presented in Figure 2. The manganese powder particles, shown in Figure 2a and b, were significantly larger than the particles of the other two reagents. They featured irregular shapes with sharp edges. At higher magnification, small, needle-shaped crystals were observed on the surfaces of the manganese. The bismuth oxide (Figure 2c) and tin (Figure 2d) particles were globular-shaped with smooth outer surfaces. Careful examination of the SEM images revealed that the small primary tin particles had some tendency to aggregate into larger grains. The bismuth trioxide also showed a tendency to aggregate with the fuel particles. This was inferred from the observation that the bulk volume increased during the brush-mixing process.

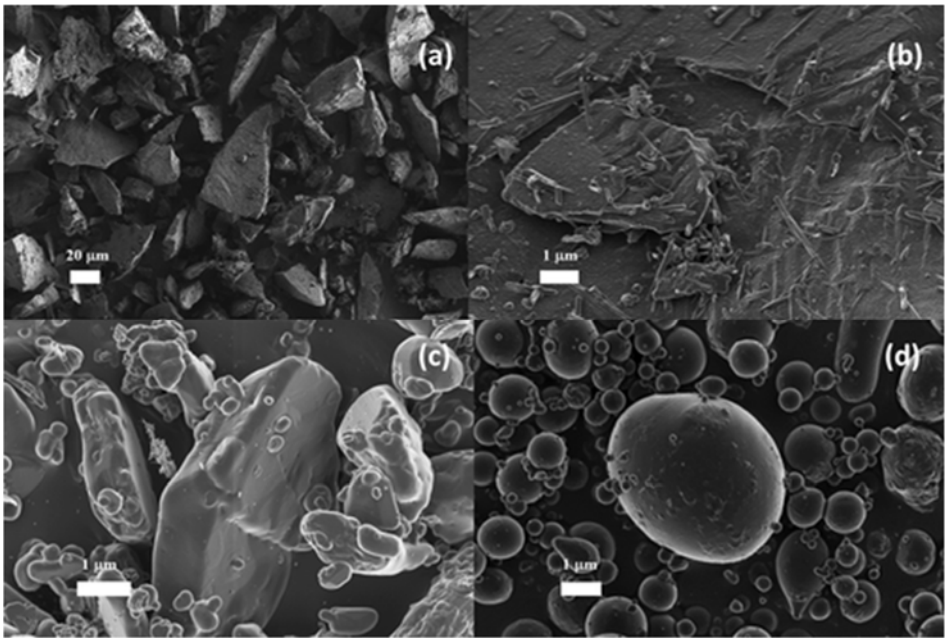


**Figure 2.** Scanning electron micrographs of the (a,b) manganese; (c) bismuth oxide, and (d) tin particles.

**Table 3. XRF Analysis of the Bismuth Oxide Powder**[a]

| $Na_2O$ | $P_2O_5$ | $K_2O$ | CaO | $TiO_2$ | $ZrO_2$ | $Bi_2O_3$ | Total |
|---|---|---|---|---|---|---|---|
| 0.167 | 1.08 | 0.016 | 0.704 | 0.010 | 0.156 | 96.05 | |
| $Ag_2O$ | SrO | $MoO_3$ | $As_2O_3$ | $Rb_2O$ | $PtO_2$ | $PuO_2$ | |
| 0.042 | 0.019 | 0.034 | 0.441 | 0.183 | 1.020 | 0.026 | 99.9 |

[a]Values are given in wt %.

The particle size, BET surface area, and density of the powders are presented in Table 1. The particle size values for the manganese powder correlate with the larger size revealed by the SEM micrographs. According to the XRF analysis in Table 3, the bismuth oxide powder contained in excess of 96% $Bi_2O_3$. The main elemental impurities present were phosphorus and, surprisingly, platinum. The X-ray diffractogram (XRD) was consistent with pure monoclinic $Bi_2O_3$, i.e., bismite. Additional information on the properties of the reagents is presented in the Supporting Information.

**Table 4. Burning Rates and Compaction Levels of Formulations Tested in Glass Tubes**

| Composition, wt % | | | Burning rate, $mm \cdot s^{-1}$ | Compaction, % | Energy output |
|---|---|---|---|---|---|
| $Bi_2O_3$ | Mn | Sn | $u \pm s$ | TMTD $\pm s$ | $MJ \cdot kg^{-1}$ |
| 75 | 0 | 25 | 12.1 ± 1.2 | 45.0 ± 0.2 | |
| 72.4 | 0 | 27.7 | 12.7 ± 0.5 | 45.0 ± 0.0 | 0.484 ± 0.008 |
| 70 | 0 | 30 | 13.7 ± 1.1 | 45.2 ± 0.8 | 0.464 ± 0.026 |
| 65 | 0 | 35 | 13.4 ± 0.6 | 45.2 ± 0.8 | 0.479 ± 0.029 |
| 60 | 0 | 40 | 9.5 ± 0.6 | 45.0 ± 0.2 | 0.444 ± 0.027 |
| 55 | 0 | 45 | 9.4 ± 0.1 | 45.3 ± 0.9 | |
| 50 | 0 | 50 | 7.0 ± 0.8 | 45.3 ± 1.0 | |
| 45 | 0 | 55 | 3.8 ± 0.7 | 45.5 ± 1.3 | |
| 75 | 25 | 0 | 8.0 ± 0.4 | 47.6 ± 0.4 | 0.95 |
| 70 | 30 | 0 | 11.2 ± 0.8 | 47.8 ± 0.4 | 1.04 |
| 65 | 35 | 0 | 8.9 ± 1.2 | 47.6 ± 0.1 | 1.15 |
| 60 | 40 | 0 | 6.3 ± 1.8 | 47.9 ± 0.1 | 0.92 |
| 56.7 | 40.5 | 2.8 | 2.9 ± 0.6 | 50.6 ± 0.4 | |
| 50 | 35 | 15 | 3.0 ± 0.1 | 51.8 ± 0.5 | |
| 56.5 | 40.5 | 3 | 3.2 ± 0.3 | 49.9 ± 0.1 | |
| 49.5 | 42.4 | 8.1 | 3.4 ± 0.3 | 50.5 ± 0.3 | 0.823 |
| 49.5 | 40.5 | 10 | 3.5 ± 0.4 | 50.5 ± 0.4 | |
| 59.3 | 33.8 | 6.9 | 3.6 ± 0.1 | 52.3 ± 2.7 | |
| 62.5 | 22.5 | 15 | 4.0 ± 0.2 | 49.7 ± 0.7 | 0.832 ± 0.023 |
| 50 | 20 | 30 | 4.0 ± 0.2 | 49.1 ± 0.3 | |
| 63.7 | 22.5 | 13.8 | 4.1 ± 0.7 | 49.6 ± 0.5 | 0.921 ± 0.030 |
| 54 | 23 | 23 | 4.4 ± 0.4 | 48.7 ± 0.2 | |
| 56 | 27 | 17 | 4.5 ± 0.1 | 48.7 ± 0.2 | |
| 50 | 30 | 20 | 4.6 ± 0.2 | 50.6 ± 0.3 | |
| 58.8 | 33.8 | 7.5 | 4.6 ± 0.9 | 50.2 ± 0.2 | 0.977 ± 0.008 |
| 56 | 17 | 27 | 5.1 ± 0.3 | 47.3 ± 0.1 | |
| 68 | 11.3 | 20.7 | 5.5 ± 0.5 | 46.7 ± 0.2 | |
| 66.3 | 11.3 | 22.5 | 6.8 ± 0.3 | 49.4 ± 0.9 | 0.788 ± 0.052 |
| 68.5 | 4.5 | 27 | 9.4 ± 0.9 | 46.3 ± 0.2 | |
| 63 | 1.9 | 35.1 | 10.5 ± 0.4 | 46.4 ± 0.3 | 0.824 ± 0.010 |
| 63 | 10 | 27 | 10.9 ± 0.8 | 46.7 ± 0.2 | |
| 50 | 10 | 40 | - | - | |
| 46 | 37 | 17 | - | - | |
| 46 | 27 | 27 | - | - | |
| 46 | 17 | 37 | - | - | |

**Burning Rate Measurements**

Table 4 lists the burning rate ($u$) values and the compaction density, expressed as the theoretical maximum density (TMD), for all the formulations tested in glass tubes. The burning rate showed highly nonlinear variation with composition. Padè mixture models are families of rational polynomials based on Scheffe K-polynomials.[21] They are eminently suitable for correlating complex mixture property behavior.[21–24] Consequently, the data was correlated using the Padè mixture model shown in eq 1

$$u = \sum_{i,j,k} a_{ijk} w_i w_j w_k / \sum_{i,j} b_{ij} w_i w_j \tag{1}$$

where $u$ is the burning rate in mm·s$^{-1}$ and the $w_i$ values are the mass fractions of the different components corresponding to the ternary system $Bi_2O_3$ (1)–Mn (2)–Sn (3). The $a_{ijk}$ and $b_{ij}$ values are adjustable model constants. In this model, the ratios $a_{iii}/b_{ii}$ indicate the contribution of component $i$ to the burning rate, while the parameters quantify interactions between the components. Note that the parameter values in this model are, in a relative sense, not completely independent variables. Therefore, the constant $b_{33}$ was assigned a value of unity to fix their relative magnitudes. The values for the other constants were established using least-squares regression, and they are reported in Supporting Information.

Figure 3 shows plots that compare the experimentally determined burning rates with predictions of the model. The mean absolute deviation was 12% and the maximum deviation was 16%. This is acceptable considering that the relative standard deviation of the measurements was ca. 10% while the maximum standard deviation was 29%. It is evident from Figure 3b that there is an outlier in the data set that was nevertheless included in the regression analysis. Both binaries feature a maximum burning rate at a $Bi_2O_3$ content of ca. 70 wt %. Compositions based on tin as the fuel burn slightly faster and over a wider stoichiometric range. The lowest burning rate measured was just 2.9 mm·s$^{-1}$.

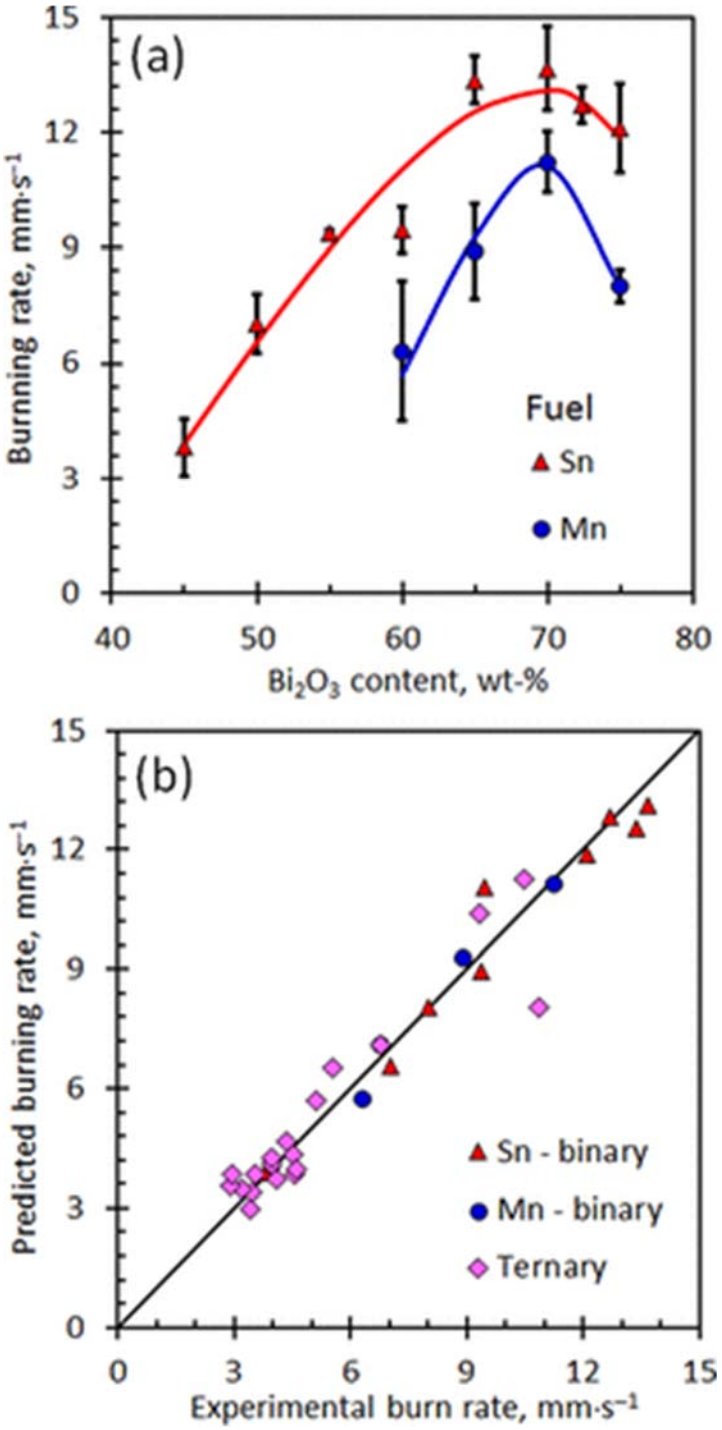


**Figure 3.** (a) Effect of the $Bi_2O_3$ content on the burning rates of binary mixtures in glass tubes with tin or manganese as fuel. (b) Comparison of the burning rates predicted by the mixture model of eq 1.

Figure 4 plots the experimental formulations that actually burned in glass tubes on a ternary composition diagram. The plotted points are color-coded depending on whether the measured burning rate was less or higher than $u$ = 5 mm·s$^{-1}$. Also shown are model-predicted contours for a constant burning rate at this value, as well as a predicted contour

for flame extinction. Interestingly, the model predicts that, with both fuels present, burning is sustained at lower oxidant concentrations than are possible with the binary systems. In addition, compositions based on mixtures of the two metal fuels also tend to burn more slowly. The actual ternary compositions tested confirmed these two conclusions. Therefore, both the experimental data and the model support the expectation that reliable burning rates lower than $u$ = 5 mm·s$^{-1}$ should be possible in this composition space.

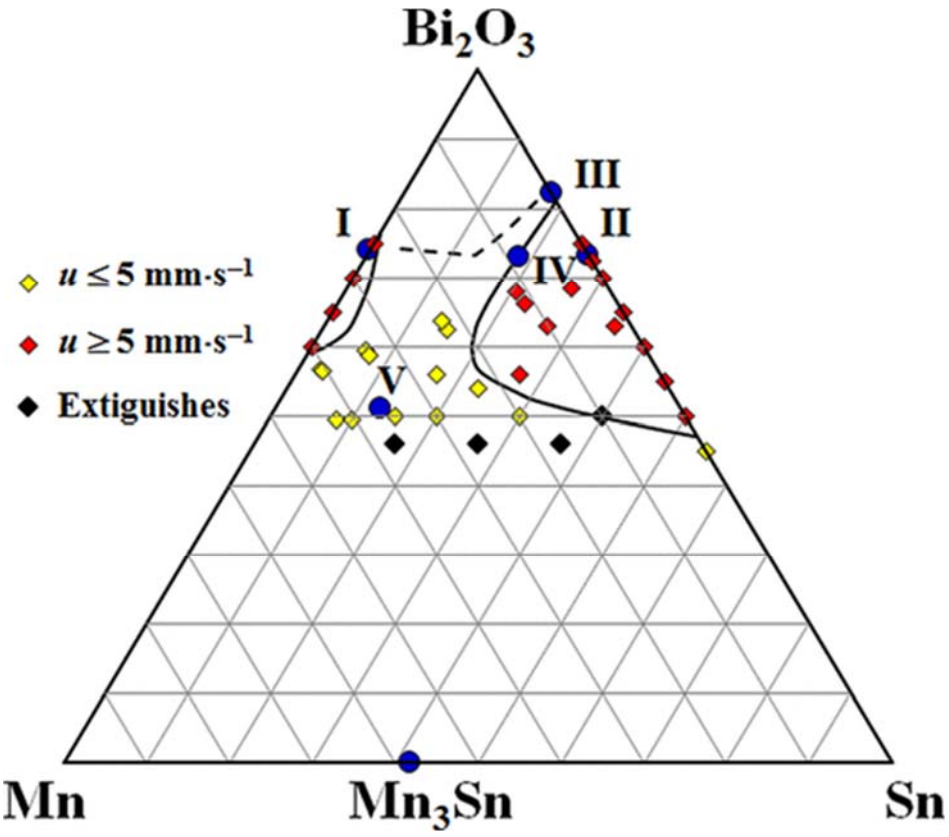


**Figure 4**. Ternary diagram plotting the experimental formulations and showing the dominant reactions. The solid and broken lines indicate model-predicted contours of constant burning rate corresponding to $u$ = 5 mm·s$^{-1}$ and $u$ = 0 mm·s$^{-1}$ (flame extinction), respectively. The Roman numerals indicate the reagent ratios corresponding to the reaction schemes shown in Table 8.

Table 5 compares burning rates obtained in lead and glass tubes. The binary compositions burnt somewhat more slowly in the glass tubes, but the opposite was the case for the ternary compositions. The reason for this difference is not currently understood.

XRD analysis on burn residues. The results of the XRD analysis performed on the burn residues is presented in Tables 6 and 7. The observed product spectra, over the range of compositions evaluated presently, are consistent with, and explained by, the five reactions presented in Table 8. MnO or $SnO_2$ are the primary products obtained on the burning of compositions A1 to A6 in Table 6. Sample A1 confirms that manganese is preferentially oxidized as the product contain MnO (but no $SnO_2$) and unreacted tin (but no unreacted manganese). The formation of the oxide products are explained by Scheme I and Scheme II. These reactions correspond to classic thermites in which the metal fuel is converted into its

**Table 5. Comparing Burning Rates Measured in Lead and Glass Tubes**

| | Formulation | A | B | C | A + C(1:1) | B + C(1:1) |
|---|---|---|---|---|---|---|
| Composition | $Bi_2O_3$ | 73.25 | 70.0 | 55.0 | 63.7 | 62.5 |
| | Mn | - | - | 45.0 | 22.5 | 22.5 |
| | Sn | 26.75 | 30.0 | - | 13.8 | 15 |
| Open burn | $u$, $mm \cdot s^{-1}$ | 60 ± 5 | 105 ± 1 | 6.6 ± 0.6 | 16 ± 4 | 18 ± 7 |
| Glass tubes | $u$, $mm \cdot s^{-1}$ | 12.7 ± 0.5 | 13.7 ± 1.1 | - | 4.13 ± 0.6 | 3.96 ± 0.2 |
| | TMTD, % | 45.1 ± 0.0 | 45.2 ± 0.6 | - | 49.6 ± 0.4 | 49.7 ± 0.2 |
| Lead tubes | $u$, $mm \cdot s^{-1}$ | 17.7 ± 1.4 | 14.5 ± 0.8 | - | 6.51 ± 1.0 | 6.45 ± 0.8 |
| | TMTD, % | 40.4 | 42.8 | - | 48.1 | 44.6 |

**Table 6. Compositions with Oxides or Metal Stannates as Products**

| | A1 | A2 | A3 | A4 | A5 | A6 | A7 | A8 | A9 | A10 | A11 |
|---|---|---|---|---|---|---|---|---|---|---|---|
| | | | | | Reagents | | | | | | |
| $Bi_2O_3$ | 62.5 | 63.7 | 72.4 | 70.0 | 60.0 | 50.0 | 68.5 | 68.0 | 66.2 | 63.0 | 63.0 |
| Mn | 22.5 | 22.5 | | | | | 4.5 | 11.3 | 11.3 | 10.0 | 5.8 |
| Sn | 15.0 | 13.8 | 27.7 | 30.0 | 40.0 | 50.0 | 27.0 | 20.7 | 22.5 | 27.0 | 31.2 |
| | | | | | Products | | | | | | |
| Bi | 51.5 | 46.1 | 33.9 | 36.7 | 43.4 | 43.9 | 45.8 | 52.0 | 30.7 | 56.9 | 46.2 |
| MnO | 41.0 | 34.6 | | | | | 1.2 | 2.1 | 2.0 | 1.1 | |
| $SnO_2$ | | | 45.1 | 46.5 | 48.5 | 29.8 | 33.8 | 12.5 | 16.6 | 7.9 | 35.1 |
| $2MnO{\cdot}SnO_2$ | | 4.9 | | | | | 10.0 | 28.5 | 46.9 | 24.6 | |
| $Bi_2O_3{\cdot}2SnO_2$ | | | 1.0 | 2.1 | 3.2 | | 2.2 | | | | 18.2 |
| | | | | | Unreacted reagents | | | | | | |
| $Bi_2O_3$ | | 5.6 | 20.0 | 14.6 | 4.9 | | 7.1 | | 0.9 | | |
| Sn | 7.5 | | | | | 26.4 | | 1.6 | | 9.4 | 0.5 |
| Mn | | | | | | | | 0.1 | | | |
| | | | | | Minor products | | | | | | |
| $Bi_{0.05}Sn_{0.95}$ | | 8.9 | | | | | | | 3.0 | | |
| $MnO{\cdot}SnO_2$ | | | | | | | | 3.3 | | | |

most stable oxide while the bismuth oxide is reduced to the metal state. At higher levels of bismuth oxide, the reaction with tin yields bismuth stannate ($Bi_2O_3 \cdot 2SnO_2$) as shown in Scheme III. This was observed for composition A11 in Table 6. In Scheme IV, the reaction of the oxidant with similar amounts of the two fuels leads to the formation of manganese stannate ($2MnO \cdot SnO_2$) instead of the two separate metal oxides. See the product spectra for compositions A7 to A10 in Table 6. Despite the existence of several manganese–tin intermetallic compounds, only $Mn_3Sn$ was actually observed as a reaction product. This compound formed when the manganese proportion in the fuel component was significantly higher than that of tin. Part of the manganese was oxidized to MnO, and the rest then reacted with the tin to form the intermetallic compound as indicated by Scheme IV in Table 8. Interestingly, samples B1 to B6 in Table 7 were among the six slowest burning compositions and all of them had the intermetallic $Mn_3Sn$ as a primary reaction product.

**Table 7. Compositions with MnO and the Intermetallic Compound $Mn_3Sn$ as Products**

| | B1 | B2 | B3 | B4 | B5 | B6 |
|---|---|---|---|---|---|---|
| | | | Reagents | | | |
| $Bi_2O_3$ | 56.5 | 56.7 | 49.5 | 58.7 | 59.3 | 49.5 |
| Mn | 40.5 | 40.5 | 40.5 | 33.8 | 33.8 | 42.4 |
| Sn | 3.0 | 2.8 | 10.0 | 7.5 | 6.9 | 8.1 |
| | | | Products | | | |
| Bi | 29.1 | 41.9 | 37.6 | 38.9 | 33.3 | 31.9 |
| MnO | 53.2 | 44.9 | 41.3 | 47.6 | 47.6 | 46.7 |
| $SnO_2$ | 1.2 | | | | 1.0 | |
| $Mn_3Sn$ | 11.5 | 13.3 | 19.3 | 12.6 | 12.0 | 18.5 |
| MnBi | 1.8 | | | 0.9 | 2.3 | 1.7 |
| | | | Unreacted reagents | | | |
| $Bi_2O_3$ | 1.5 | | | | 1.4 | |
| Sn | 1.3 | | | | 1.1 | |
| Mn | 0.4 | | 1.8 | | 1.4 | 1.2 |

**Table 8. Dominant Reactions Inferred from the Quantitative XRD Results**

| | | Reagents, wt % | | |
|---|---|---|---|---|
| Scheme | Reaction | $Bi_2O_3$ | Mn | Sn |
| I | $Bi_2O_3 + 3Mn \rightarrow 3MnO + 2Bi$ | 73.87 | 26.13 | - |
| II | $2Bi_2O_3 + 3Sn \rightarrow 4Bi + 3SnO_2$ | 72.35 | - | 26.75 |
| III | $7Bi_2O_3 + 6Sn \rightarrow 3Bi_2O_3 \cdot 2SnO_2 + 8Bi$ | 82.08 | - | 17.92 |
| IV | $Bi_2O_3 + Mn + Sn \rightarrow 2Bi + MnO \cdot SnO_2$ | 72.85 | 8.59 | 18.56 |
| V | $Bi_2O_3 + 5Mn + Sn \rightarrow 2Bi + 2MnO + Mn_3Sn$ | 50.96 | 36.05 | 12.98 |

**Bomb Calorimeter Results**

Table 4 also lists the energy outputs, measured with the bomb calorimeter, for selected compositions. In the oxidant range considered, the energy of reaction (U) for the $Bi_2O_3$/Sn binary was approximately constant. It varied from about 0.44 to 0.48 $MJ \cdot kg^{-1}$ as the oxidant content increased from 55 to ca. 72 wt %. The exothermicity of the $Bi_2O_3$/Mn binary over a similar oxidant range is about double this value.[16]The values measured for the ternary compositions reported in Table 4 are close to those for the $Bi_2O_3$/Mn binary. This suggests that, when both fuels are present, secondary exothermic reactions occur, e.g., reactions IV and V in Table 8. The intermetallic reaction (V) between the manganese and the tin is important at low oxidant and relatively high manganese levels. The manganese reduces the bismuth oxide and the excess reacts with the tin present. Manganese stannate forms at high bismuth oxide contents when the metal fuels are present at near-equimolar quantities. These reactions allow the design of slow-burning composition by maintain the exothermicity at adequate levels.

## Conclusions

Slow-burning pyrotechnic compositions were found in the ternary system comprising bismuth oxide as oxidant and manganese and tin as the fuels. The binary systems behaved as expected for standard thermite reactions in which the bismuth oxide is reduced to the metal and the oxide MnO or $SnO_2$ are formed. The reaction products in the ternary system depend strongly on the relative proportions of the reagents. Manganese is preferentially oxidized in comparison to tin. If sufficient oxidizer is present, both fuels are oxidized and manganese stannate forms instead of the separate metal fuel oxides. At low manganese and very high $Bi_2O_3$ contents, the formation of bismuth stannate was observed. At high manganese to bismuth ratios and low oxidizer contents, the intermetallic compound $Mn_3Sn$ was formed. The slowest burning compositions were those associated with the formation of this intermetallic compound.

## Acknowledgments

This work is based on research that was supported by the University of Pretoria through a PhD stipend awarded to S. Guo.

**Abbreviations**

| | | | |
|---|---|---|---|
| TMD | theoretical | TMD | theoretical |
| XRD | X-ray diffrac | XRD | X-ray diffrac |

## References

**1.** Bradley, J. N.; Capey, W. D.; Shere, J. F. Mechanism of Reaction in Metal+Metal Oxide Systems. *Nature* **1979**, *277* (5694), 291– 292, DOI: 10.1038/277291a0

**2**. Conkling, J. A. Pyrotechnics. In *Kirk-Othmer Encyclopedia of Chemical Technology (Ed.)*; John Wiley & Sons, Inc.: 2000. DOI: 10.1002/0471238961.1625181503151411.a01

**3**. Hardt, A. P.; Phung, P. V. Propagation of Gasless Reactions in Solids-I. Analytical Study of Exothermic Intermetallic Reaction Rates. *Combust. Flame* **1973**, *21* (1), 77– 89, DOI: 10.1016/0010-2180(73)90009-6

**4**. Puszynski, J.; Degreve, J.; Hlavacek, V. Modeling of Exothermic Solid-Solid Noncatalytic Reactions. *Ind. Eng. Chem. Res.* **1987**, *26* (7), 1424– 1434, DOI: 10.1021/ie00067a026

**5**. McLain, J. H. *Pyrotechnics from the Viewpoint of Solid State Chemistry*; Franklin Institute Press: Philadelphia, PA, 1980.

**6**. Beck, M. W.; Flanagan, J. Delay Composition and Device. US Patent 5147476A, 1992.

**7.** Charsley, E. L.; Chen, C.-H.; Boddington, T.; Laye, P. G.; Pude, J. R. G. Differential Thermal Analysis and Temperature Profile Analysis of Pyrotechnic Delay Systems: Ternary Mixtures of Silicon, Boron and Potassium Dichromate. *Thermochim. Acta* **1980**, *35* (2), 141– 152, DOI: 10.1016/0040-6031(80)87188-7

**8**. Berger, B. Parameters Influencing the Pyrotechnic Reaction. *Propellants, Explos., Pyrotech.* **2005**, *30* (1), 27– 35, DOI: 10.1002/prep.200400082

**9**. Focke, W. W.; Tichapondwa, S. M.; Montgomery, Y. C.; Grobler, J. M.; Kalombo, M. L. Review of Gasless Pyrotechnic Time Delays. *Propellants, Explos., Pyrotech.* **2019**, *44* (1), 55– 93, DOI: 10.1002/prep.201700311

**10**. Tchounwou, P. B.; Yedjou, C. G.; Patlolla, A. K.; Sutton, D. J. Heavy Metal Toxicity and the Environment. *EXS* **2012**, *101*, 133– 164, DOI: 10.1007/978-3-7643-8340-4_6

**11**. Steinhauser, G.; Klapötke, T. M. Green" Pyrotechnics: A Chemists' Challenge. *Angew. Chem., Int. Ed.* **2008**, *47* (18), 3330– 3347, DOI: 10.1002/anie.200704510

**12**. Sabatini, J. J. Advances Toward the Development of "Green" Pyrotechnics. In *Green Energetic Materials*, Brinck, T., Ed.; John Wiley & Sons, Ltd., 2014; pp 63– 102. DOI: 10.1002/9781118676448.ch04 .

**13**. Ma, X.; Li, Y.; Hussain, I.; Shen, R.; Yang, G.; Zhang, K. Core–Shell Structured Nanoenergetic Materials: Preparation and Fundamental Properties. *Adv. Mater.* **2020**, *32* (30), 2001291, DOI: 10.1002/adma.202001291

**14**. Montgomery, Y. C.; Focke, W. W.; Atanasova, M.; Del Fabbro, O.; Kelly, C. Mn+$Sb_2O_3$ Thermite/Intermetallic Delay Compositions. *Propellants, Explos., Pyrotech.* **2016**, *41* (5), 919– 925, DOI: 10.1002/prep.201600007

**15.** Guo, S.; Focke, W. W.; Tichapondwa, S. M. Al-Ni-NiO Pyrotechnic Time-Delays. *Propellants, Explos., Pyrotech.* **2020**, *45* (4), 665– 670, DOI: 10.1002/prep.201900304

**16**. Tichapondwa, S. M. Burn Properties of the Mn/$Bi_2O_3$ Pyrotechnic Time Delay Composition, 2020; Submitted for publication.

**17.** Howe, P.; Watts, P. *Concise International Chemical Assessment Document 65. Tin and inorganic tin compounds*; World Health Organization: Geneva, 2005; pp 1– 73.

**18**. Mohan, R. Green bismuth. *Nat. Chem.* **2010**, *2* (4), 336, DOI: 10.1038/nchem.609

**19**. DiPalma, J. R. Bismuth Toxicity, Often Mild, Can Result in Severe Poisonings. *Emerg. Med. News* **2001**, *23* (3), 16, DOI: 10.1097/00132981-200104000-00012

**20**. Shaw, A. P. G. *Thermitic Thermodynamics: A Computational Survey and Comprehensive Interpretation of Over 800 Combinations of Metals, Metalloids, and Oxides*; CRC Press: Boca Raton, Florida, USA, 2020; pp 674 and 937.

**21**. Focke, W. W.; Du Plessis, B. Correlating Multicomponent Mixture Properties with Homogeneous Rational Functions. *Ind. Eng. Chem. Res.* **2004**, *43* (26), 8369– 8377, DOI: 10.1021/ie049415+

**22**. Focke, W. W. Mixture Model for Correlating Excess Enthalpy Data. *J. Chem. Eng. Jpn.* **2007**, *40* (4), 295– 303, DOI: 10.1252/jcej.40.295

**23**. Focke, W. W. Correlating Thermal-Conductivity Data for Ternary Liquid Mixtures. *Int. J. Thermophys.* **2008**, *29* (4), 1342– 1360, DOI: 10.1007/s10765-008-0465-2

**24.** Focke, W. W.; Ackermann, M. H.; Coetzer, R. L. J. Mixing Rules Based on Power Means and Generalized q-Fractions. *J. Chem. Eng. Jpn.* **2012**, *45* (1), 1– 8, DOI: 10.1252/jcej.11we003